New Improved Model and Accurate Analytical Response of SiPMs Coupled to Read-Out Electronics

Davide Marano, Giovanni Bonanno, Salvatore Garozzo, Alessandro Grillo, and Giuseppe Romeo

***Abstract*— In this letter, a recently published model of silicon photomultiplier (SiPM) sensors is profitably extended to include the important effects of the read-out electronics on the shape of the output pulse waveforms. An improved analytical expression has been developed, also accounting for the loading effect and bandwidth limitation of the coupled front-end, through which the SiPM dynamic response can be accurately reproduced and predicted. Experimental tests on actual detection systems corroborate the SiPM model and the analytical results.**

***Index Terms*— Analytical model, dynamic response, front-end electronics, pulse waveform, SiPM sensors.**

I. Introduction

SILICON photomultiplier sensors (SiPM) have been recently gaining widespread diffusion within the fields of high-energy physics, nuclear medicine, and astrophysics.

The rising number of perspective applications requiring optimal dynamic speed and single photon time resolution, along with the ensuing demand for suitable integrated front-end systems, have provided research motivation for accurate analytical studies on the SiPM response to incident photons [1]–[6].

Knowledge and prediction of the output pulse shape is crucial for an optimal design of SiPM read-out architectures, allowing designers to select the best characteristics of the front-end electronics for optimizing overall time performance based on specific application requirements.

This letter improves and completes the analytical investigation of the SiPM dynamic response in [1], accounting for the loading effect and bandwidth restriction of the coupled read-out electronics, that may sensibly affect single photoelectron resolution and timing capabilities of the detection system.

II. Improved SiPM Analytical Model

The equivalent electrical circuit of a SiPM sensor coupled to the front-end electronics is depicted in Fig. 1.

The SiPM model is able to simulate the discharge of N_f active pixels over a number N of total microcells. The circuit

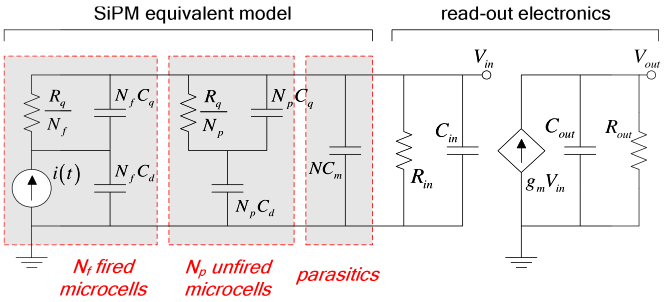

Fig. 1. Complete electrical model of SiPM and front-end electronics.

is divided into an active component for the N_f fired pixels and a passive part for the $N_p = N - N_f$ unfired microcells. For a single cell, C_d is the junction capacitance of the inner depletion layer, R_q and C_q are respectively the quenching resistance and stray capacitance, and C_m accounts for the parasitic interconnect capacitance across the SiPM terminals.

The equivalent circuit of the front-end electronics relies on the traditional single-pole system model of a generic read-out pre-amplifier, where R_{in} and C_{in} are respectively the amplifier equivalent input resistance and capacitance, $g_m R_{out}$ is the DC gain, whilst $R_{out}C_{out}$ is the reciprocal of the -3dB cut-off frequency resulting from dominant-pole approximation.

Avalanche discharges of the firing cells are modeled by the current source $i(t)$, which abruptly reaches its peak amplitude I_0, depending on the excess bias voltage V_{OV} over breakdown, and exponentially drops with a circuit-dependent decay time constant τ_d. For a single fired cell, $i(t)$ can be expressed by

$$i(t) \approx I_0 e^{-\frac{t}{\tau_d}} = \frac{V_{OV}}{R_d} e^{-\frac{t}{R_d(C_d+C_q)}}, \tag{1}$$

where R_d is the inner resistance of the space-charge regions.

The trans-resistive small-signal transfer function of the circuit in Fig. 1 as a function of the complex frequency s is

$$F(s) = \frac{V_{out}(s)}{I(s)} = A\frac{1 + b_1 s}{\left(1 + a_1 s + a_2 s^2\right)(1 + a_0 s)}, \tag{2}$$

with $A = g_m R_{in} R_{out}$, $b_1 = R_q C_q$, $a_0 = R_{out} C_{out}$, and

$$a_1 = R_q\left(C_d + C_q\right) + R_{in}\left[C_{in} + N\left(C_d + C_m\right)\right], \tag{3}$$

$$a_2 = R_{in} R_q\left[NC_d C_q + \left(C_{in} + NC_m\right)\left(C_d + C_q\right)\right]. \tag{4}$$

Being $a_1^2 > 4a_2$ for any values of the passive elements, the above transfer function can be rewritten as

$$F(s) = A\frac{1 + s\tau_z}{\left(1 + s\tau_{p1}\right)\left(1 + s\tau_{p2}\right)(1 + s\tau_{out})}, \tag{5}$$

in which $\tau_z = b_1$, $\tau_{out} = a_0$, and

$$\tau_{p1}, \tau_{p2} = \frac{1}{2}\left(a_1 \pm \sqrt{a_1^2 - 4a_2}\right). \tag{6}$$

Manuscript received May 28, 2015; revised July 13, 2015; accepted July 31, 2015. Date of publication August 3, 2015; date of current version December 10, 2015. This work was supported in part by the ASTRI Flagship Project, financed by the Italian Ministry of Education, University and Research (MIUR) and led by the Italian National Institute for Astrophysics (INAF). The associate editor coordinating the review of this letter and approving it for publication was Prof. Zeljko Ignjatovic.

The authors are with INAF, Osservatorio Astrofisico di Catania, Catania I-95123, Italy (e-mail: davide.marano@oact.inaf.it; giovanni.bonanno@oact.inaf.it; salvatore.garozzo@oact.inaf.it; alessandro.grillo@oact.inaf.it; giuseppe.romeo@oact.inaf.it).

Color versions of one or more of the figures in this letter are available online at http://ieeexplore.ieee.org.

Digital Object Identifier 10.1109/JSEN.2015.2464077

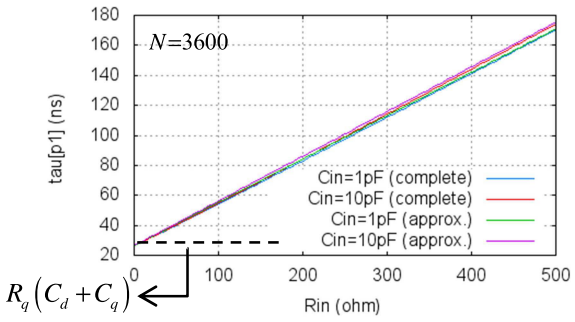

Fig. 2. Complete and approximated analytical expressions of the SiPM recharging time constant τ_{p1} as a function of the front-end input resistance R_{in} and for different values of the input capacitance C_{in}.

Solving (2) for $V_{out}(s)$, substituting the s-domain expression of $i(t)$ in (1), and then inverse Laplace transforming, the final SiPM transient response is derived as follows

$$v_{out}(t) = k\left(A_d e^{-\frac{t}{\tau_d}} + A_{p1} e^{-\frac{t}{\tau_{p1}}} + A_{p2} e^{-\frac{t}{\tau_{p2}}} + A_{out} e^{-\frac{t}{\tau_{out}}}\right), \tag{7}$$

with $k = AI_0\tau_d$, and the four exponentials coefficients given by

$$A_d = \frac{\tau_d(\tau_d - \tau_z)}{(\tau_d - \tau_{p1})(\tau_d - \tau_{p2})(\tau_d - \tau_{out})}, \tag{8}$$

$$A_{p1} = \frac{\tau_{p1}(\tau_{p1} - \tau_z)}{(\tau_{p1} - \tau_d)(\tau_{p1} - \tau_{p2})(\tau_{p1} - \tau_{out})}, \tag{9}$$

$$A_{p2} = \frac{\tau_{p2}(\tau_{p2} - \tau_z)}{(\tau_{p2} - \tau_d)(\tau_{p2} - \tau_{p1})(\tau_{p2} - \tau_{out})}, \tag{10}$$

$$A_{out} = \frac{\tau_{out}(\tau_{out} - \tau_z)}{(\tau_{out} - \tau_d)(\tau_{out} - \tau_{p1})(\tau_{out} - \tau_{p2})}. \tag{11}$$

The new SiPM output response is a quadruple-exponential function that truly reproduces the typical rising (τ_d), quenching (τ_{p2}), and recovery (τ_{p1}) phases of the generated pulse, including the contribution of the front-end electronics.

For $\tau_{out} = 0$, as easily provable, A_d, A_{p1}, A_{p2} and $v_{out}(t)$ expressions in (7)-(11) reduce to the relevant ones in [1].

Comparing denominators of (2) and (5) leads to $a_1 = \tau_{p1} + \tau_{p2}$ and $a_2 = \tau_{p1}\tau_{p2}$, from which, assuming $\tau_{p1} \gg \tau_{p2}$ yields $\tau_{p1} \approx a_1$ and $\tau_{p2} \approx a_2/a_1$. Thus, neglecting C_m, a useful estimation of τ_{p1} is

$$\tau_{p1} \approx R_q(C_d + C_q) + R_{in}(C_{in} + NC_d). \tag{12}$$

The complete and approximated expressions of τ_{p1}, respectively in (6) and (12), as a function of the front-end input resistance and for different values of the input capacitance, are plotted in Fig. 2, which shows a roughly linear growth of the SiPM recharging time constant as a function of R_{in}, with marginal deviations versus C_{in}.

In Fig. 3 the SiPM output voltage $v_{out}(t)$ is plotted upon the same pre-amplifier gain and different cut-off frequencies and input resistances, for a single firing cell and typical parameter values. The rise time and peak amplitude of the output pulse are found to be directly affected by the electronics

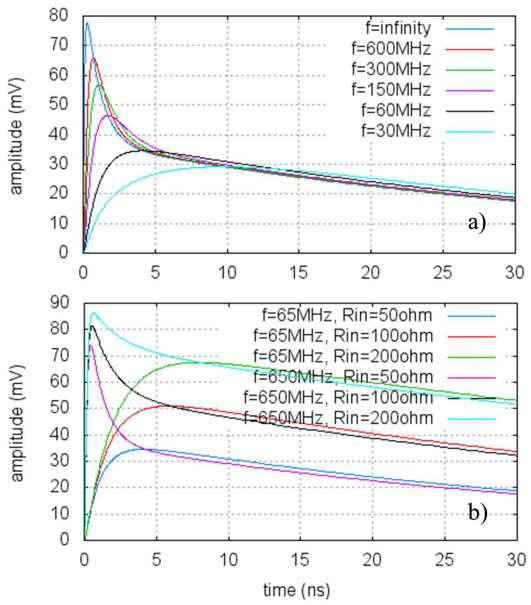

Fig. 3. Analytical SiPM output pulses: a) for $R_{in} = 50\Omega$ and different values of the pre-amplifier bandwidth f, and b) for two different bandwidths and rising values of R_{in} ($V_{OV} = 0.88$V, $N = 3600$, $R_d = 1$kΩ, $R_q = 300$kΩ, $C_d = 80$fF, $C_q = 10$fF,$C_m = 1$fF, $C_{in} = 1$pF, $g_m R_{out} = 350$).

bandwidth, f. Also, the rise time is almost independent of R_{in}, while *the functional relationship between the peak amplitude and R_{in} is strongly dependent on f, i.e., the higher the bandwidth is, the lower the pulse peak increases with R_{in}*; ideally, for $f \to \infty$, the peak value is verified to be almost independent of R_{in}.

In addition, the charge released by the fired pixels, which is proportional to the area underneath the curves, is independent of τ_{out}, and thus is not affected by the amplifier bandwidth.

The above results are believed to be particularly important, especially for the growing number of applications demanding best theoretical time performance, dynamic range, and photon number resolution of the whole detection system.

III. Experimental Model Validation

To confirm the effectiveness of the achieved results, simulations and laboratory measurements are carried out on physical devices and different read-out systems with known characteristics. Analytical and measured output time responses to a dark pulse are compared for a 3×3-mm^2 Hamamatsu detector, featuring a 50-μm cell size and 3600 pixels. Tests are performed at room temperature, using two voltage pre-amplifiers with 300-MHz and 50-MHz nominal closed-loop bandwidths and equal 50-Ω input resistance. Calibrated cabling systems are used to minimize coupling inductances and capacitances.

Model parameters are assessed based on experimental tests performed through specific characterization protocols [7], [8].

Model parameters of the read-out section in Fig. 1 are obtained from the knowledge of the specific amplifier adopted. The input capacitance C_{in} is available from the manufacturer datasheet, and the input and output resistances, R_{in} and R_{out} respectively, along with the –3dB small-signal bandwidth f are obtained from the simulation model once the desired amplifier configuration and closed-loop gain A are selected.

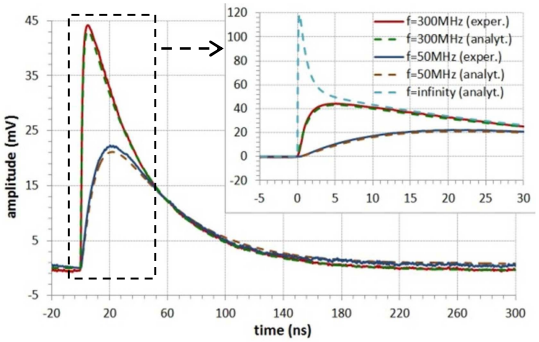

Fig. 4. Analytical and experimental (averaged) SiPM dark output responses using two read-out voltage pre-amplifiers with different bandwidths.

So, from equation $A = g_m R_{out}$ parameter g_m is derived, while the value of C_{out} is extracted through the expression $f = 1/(2\pi R_{out} C_{out})$.

For a single dark pulse, data outputs of both analytical and experimental voltage pulses are merged in Fig. 4 for the same pre-amplifier gain factor. As inspected, a good curve fitting is obtained, thus cross-checking the developed analysis. The inset plot in Fig. 4 also shows the ideal response for $f \to \infty$.

IV. Conclusion

In this contribution, the validity of a previously presented SiPM analytical model is extended to account for the characteristics of the read-out electronics. It is confirmed that both loading effects and bandwidth restrictions play a relevant role in the determination of the output pulse shape.

References

[1] D. Marano *et al.*, "Accurate analytical single-photoelectron response of silicon photomultipliers," *IEEE Sensors J.*, vol. 14, no. 8, pp. 2749–2754, Aug. 2014.

[2] F. Corsi *et al.*, "Electrical characterization of silicon photo-multiplier detectors for optimal front-end design," in *Proc. IEEE Nucl. Sci. Symp. Conf. Rec.*, Oct./Nov. 2006, pp. 1276–1280.

[3] A. K. Jha, H. T. van Dam, M. A. Kupinski, and E. Clarkson, "Simulating silicon photomultiplier response to scintillation light," *IEEE Trans. Nucl. Sci.*, vol. 60, no. 1, pp. 336–351, Feb. 2013.

[4] G. Giustolisi, G. Palumbo, P. Finocchiaro, and A. Pappalardo, "A simple extraction procedure for determining the electrical parameters in silicon photomultipliers," in *Proc. IEEE ECCTD*, Sep. 2013, pp. 1–4.

[5] D. Marano *et al.*, "Silicon photomultipliers electrical model extensive analytical analysis," *IEEE Trans. Nucl. Sci.*, vol. 61, no. 1, pp. 23–34, Feb. 2013.

[6] D. Marano *et al.*, "Improved SPICE electrical model of silicon photomultipliers," *Nucl. Instrum. Methods Phys. Res. A, Accel. Spectrom. Detect. Assoc. Equip.*, vol. 726, pp. 1–7, Oct. 2013.

[7] G. Bonanno *et al.*, "Characterization measurements methodology and instrumental set-up optimization for new SiPM detectors—Part I: Electrical tests," *IEEE Sensors J.*, vol. 14, no. 10, pp. 3557–3566, Oct. 2014.

[8] G. Bonanno *et al.*, "Characterization measurements methodology and instrumental set-up optimization for new SiPM detectors—Part II: Optical tests," *IEEE Sensors J.*, vol. 14, no. 10, pp. 3567–3578, Oct. 2014.